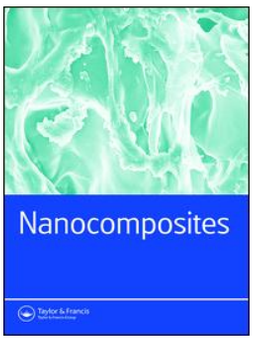

Nanocomposites

ISSN: (Print) (Online) Journal homepage: https://www.tandfonline.com/loi/ynan20

Structure and properties of thermomechanically processed silk peptide and nanoclay filled chitosan

Pei Chen , Fengwei Xie , Fengzai Tang & Tony McNally

To cite this article: Pei Chen , Fengwei Xie , Fengzai Tang & Tony McNally (2020): Structure and properties of thermomechanically processed silk peptide and nanoclay filled chitosan, Nanocomposites, DOI: 10.1080/20550324.2020.1820796

To link to this article: https://doi.org/10.1080/20550324.2020.1820796

Published online: 18 Sep 2020.

NANOCOMPOSITES
https://doi.org/10.1080/20550324.2020.1820796

Taylor & Francis
Taylor & Francis Group

Structure and properties of thermomechanically processed silk peptide and nanoclay filled chitosan

Pei Chen[a,b], Fengwei Xie[b,c]*, Fengzai Tang[d] and Tony McNally[b]

[a]College of Food Science, South China Agricultural University, Guangzhou, Guangdong, China; [b]International Institute for Nanocomposites Manufacturing (IINM), WMG, University of Warwick, Coventry, United Kingdom; [c]School of Chemical Engineering, The University of Queensland, Brisbane, Australia; [d]WMG, University of Warwick, Coventry, United Kingdom

ABSTRACT

While chitosan has great potential for biomedical and wider application due to its appealing characteristics such as biocompatibility and inherent antimicrobial activity, its properties usually need to be further tailored for specific uses. In this study, the effect of inclusion of silk peptide (SP) and nanoclays (montmorillonite, MMT and sepiolite, SPT) on the properties of thermomechanically processed chitosan were examined. Blending SP with chitosan led to a material with greater elasticity and surface wettability. For the chitosan matrix, addition of either MMT or SPT resulted in increased mechanical properties with MMT being more effective, likely due to its 2D layered structure. For the chitosan/SP matrix, while inclusion of MMT caused increased mechanical properties and thermal stability, SPT was more effective than MMT at reducing surface hydrophilicity and SPT fully counteracted the increased surface hydrophilicity caused by SP. Thus, this work shows the different effects of MMT and SPT on chitosan-based materials and provides insights into achieving balanced properties.inclusion of

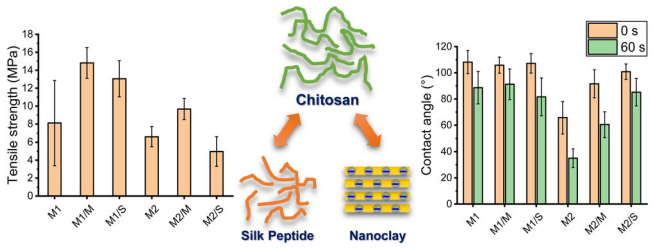

ARTICLE HISTORY
Received 14 July 2020
Accepted 3 September 2020

KEYWORDS
Chitosan; silk peptide; nanoclay; biopolymer blends; biopolymer nanocomposites; mechanical properties; surface hydrophilicity

1. Introduction

Natural biopolymers such as cellulose, chitin, proteins, starch, and alginate are widely available, safe, biocompatible, and biodegradable. The keen interest aroused in utilizing these biopolymers has been motivated by the intention to achieve greater harmony between the environment and human activities. Moreover, biopolymers also have unique characteristics, with potential in value-added applications [1–3]. For example, chitosan has a structure similar to glycosaminoglycans, is non-toxic, and has inherent antimicrobial activity and minimal foreign body reactions, and thus good wound healing properties [4].

The blending of different biopolymers has been considered to be one of the most cost-effective methods to modify the bulk properties of individual biopolymers and achieve enhanced and/or new material properties and functionality, thus, expanding the application of biopolymer materials [5,6]. For example, there has been increasing interest in the creation of new materials with tailored structure and properties based on chitosan and silk fibroin (SF). Increasing the SF/chitosan ratio increases ultimate tensile strength and elastic modulus but decreases the water storage capacity of the blended biopolymer scaffolds [4]. Research [7–11] has demonstrated that chitosan and SF, when combined, can be fabricated into biocompatible porous/sponge/fibrous materials for tissue engineering, whereas each when used alone form poor biological scaffolds. Chitosan/silk fibroin (SF) blend films can be used as a wound dressing and artificial skin because

CONTACT Fengwei Xie d.xie.2@warwick.ac.uk; Tony McNally t.mcnally@warwick.ac.uk International Institute for Nanocomposites Manufacturing (IINM), WMG, University of Warwick, Coventry CV4 7AL, United Kingdom
*This author leads the research.

of its good mechanical properties and water vapor and oxygen permeability [12].

The interfacial interactions between different biopolymers determine the structure and properties of the resulting blend or composite material. Studies [9,13,14] have suggested that strong hydrogen-bonding interactions can occur between chitosan and SF. To establish increased hydrogen bonding between chitosan and SF, more sophisticated techniques have been used to prepare layer-by-layer deposited chitosan–SF films, which showed outstanding mechanical properties [15,16]. While studies on biopolymer materials have predominantly relied on solution processing methods, which are time- and energy-intensive, thermomechanical processing is more cost-effective for the processing of biopolymers (e.g. chitosan [17–19] and alginate [20]). However, research on the thermomechanical processing of biopolymers is still extremely limited.

In this work, using thermomechanical processing techniques, we developed new composite materials based on chitosan, a low-molecular-mass silk fibroin (i.e. silk peptide, or SP) and two naturally occurring nanoclays (montmorillonite, MMT, in the form of two-dimensional (2D) nanoplatelets and sepiolite, SPT, in the form of one-dimensional (1D) nanoneedles). Low molecular mass renders SP water-soluble and easier to process. Thermomechanical processing of highly viscous materials can effectively enhance molecular interactions between chitosan and SP, leading to a more homogeneous system. Under mild acid conditions, chitosan becomes positively charged due to the protonation of the amine group [19,21]. The two nanoclays are negatively charged in their natural forms due to isomorphic substitutions occurring in the interlayer spacing between clay platelets [22,23]. Therefore, ionic interaction between chitosan and the nanoclays is expected [24,25], facilitating the dispersion of the nanoclays in the chitosan matrix. The purpose of this study is to investigate how SP and nanoclays (having different shapes) can modify the structure and properties of thermomechanically processed chitosan materials.

2. Experimental section

2.1. Materials

Chitosan (poly(β-(1,4)-D-glucosamine), derived from crab shells, with a degree of deacetylation of >90%, and a viscosity of about 100 mPa·s (1% solution in 1% acetic acid at 25 °C), a weight-average molar mass (M_w) of about 1,50,000 g mol^{-1}, was purchased from Shanghai Ryon Biological Technology Co., Ltd (China). SP powder, originally from *Bombyx mori*, with an M_w of 500–30,000 g mol^{-1}, was supplied by Huzhou Xintiansi Bio-tech Co., Ltd (China). MMT K 10 (surface area 220–270 m^2/g) and SPT were acquired from Sigma-Aldrich Company Ltd (UK); Formic acid (98% w/w AR), NaOH concentrate, and NaBr (pure) from Scientific Laboratory Supplies Ltd (UK); Methanol (technical grade) and toluene (AR) from Fisher Scientific UK Ltd. Deionized water was used in all experiments.

Table 1. Sample codes and compositions (represented as portions by weight).

Sample code	Chitosan	SP	MMT	SPT
M1	100	0	–	–
M1/M	100	0	1.5	
M1/S	100	0	–	1.5
M2	50	50	–	–
M2/M	50	50	1.5	–
M2/S	50	50	–	1.5

2.2. Sample preparation

A range of samples were prepared and the respective formulations and codes are shown in Table 1. MMT or SPT was dispersed in 30 mL of water in a small vial, which was treated with ultrasound using a tip-type sonicator (200 W, 24 kHz) for 10 min. Chitosan and/or SP (total weight 100 g) were pre-blended using an overhead stirrer for 20 min during which a mixture of 300 mL 0.5 M formic acid solution (pH = 2.03) and 30 mL of the nanoclay suspension was added dropwise. This mixture was absorbed by the biopolymers. The acid results in the protonation of the amino group of chitosan (leading to a positive charge) and disrupts the hydrogen bonding between chitosan chains [19,21]. Then, the pre-blended mixtures were stored hermetically overnight in a fridge before thermomechanically mixed and compression molded. In the sample codes, 'M1' refers to when chitosan only was the matrix while 'M2' indicates the matrix was chitosan/SP; 'M' and 'S' represents 'MMT' and 'SPT', respectively.

The thermal kneading was carried out at a temperature of 80 °C using a HAAKE Rheomix OS batch mixer (Thermo Fisher Scientific, Waltham, MA, USA) with counter-rotating rotors operating at a speed of 30 rpm for 15 min. The thermally kneaded materials were then hot-pressed into films using a COLLIN P200 P/M platen press (COLLIN Lab and Pilot Solutions GmbH, Ebersberg, Germany). The mold used had an interior size of 100 mm × 100 mm and a thickness of 1 mm. The conditions used for hot pressing were, firstly holding at 80 °C and 200 bar for 10 min, followed by cooling to room temperature (RT) for 5 min. Then, the hot-pressed films were soaked in methanol for 3 h, and then in 0.5 M NaOH solution for one day, followed by thorough washing with distilled water to remove residual chemicals. Methanol may allow SP to undergo conformational changes (i.e. the formation of β-sheets, possibly leading to enhanced mechanical properties and reduced hydrophilicity);

and NaOH solution could neutralize the acid and enhance the biopolymer mechanical properties [26].

The sheets obtained were cut into Type V dumbbell-shaped specimens according to ASTM Standard D638-14. All specimens were stored in desiccators maintained at 57% relative humidity (RH) using saturated NaBr for 3 weeks before characterization. Toluene was placed in an open beaker, which was then placed in the desiccator to prevent the samples from becoming moldy.

It was not possible to make films based on SP alone, as it became a low-viscosity gel after processing. We also tried SF (M_w about 250,000 g mol^{-1}, from the same supplier) instead of SP for processing alone or blending with chitosan but plasticized materials could not be achieved using the same processing methodology.

2.3. Characterization

Scanning electron microscopy (SEM) imaging was undertaken using a ZEISS SIGMA field-emission FEG-SEM (Carl Zeiss AG, Oberkochen, Germany) with an acceleration voltage of 2 kV for chitosan and SP powders or 6 kV for the processed biopolymer-based films. Films were first cryo-fractured using liquid nitrogen and sputter-coated with Au/Pd before examination.

Transmission electron microscopy (TEM) imaging was performed using a Talos F200X microscope (Thermo Fisher Scientific, Waltham, MA, USA) on ribbons of 60 nm thick sectioned from epoxy-embedded sample blocks. The instrument was equipped with an extreme Schottky field emission gun and a Super-X EDS (energy-dispersive X-ray spectrometry) system with integration of four silicon drift detectors. Scanning TEM (STEM) mode was operated at 200 kV with a screen current typically down to about 0.2 nA to minimize sample drifting effects. High-angle annular dark field (HAADF) images and bright field (BF) images were simultaneously acquired using Velox imaging software.

X-ray diffraction (XRD) was carried out using a PANalytical Empyrean X-ray diffractometer (Malvern Panalytical Ltd, Malvern, UK) with a Co target (Kα = 1.790307 Å) and a PIXcel1D (RTMS type) detector at 40 kV and 40 mA. Data was recorded for an angular range $2\theta = 6$–$40°$, with a step size of 0.0263° and a total scan time of 46 min.

Fourier-transform infrared (FTIR) spectra were recorded using a Bruker TENSOR 27 FTIR spectrometer (Bruker Corporation, Billerica, MA, USA) with an attenuated total reflectance (ATR) accessory. For each spectrum, 32 scans were recorded over the range of 4000–500 cm^{-1} at RT (about 22 °C) at a resolution of 4 cm^{-1}, co-added and Fourier-transformed. The background spectrum was recorded in air and subtracted from the sample spectra.

Tensile tests were performed using an Instron 3367 universal testing machine with a 1 kN load cell. A low constant crosshead speed of 3 mm/min was used due to the brittle nature of the biopolymer films [26]. As the specimens were in the form of thin sheets, specimen extension was measured by grip separation as recommended in ASTM Standard D882. Young's modulus (E), tensile strength (σ_t), and elongation at break (ε_b) were automatically determined with slack correction using Instron Bluehill 3 software from at least seven replicates of each sample.

A Mettler Toledo TGA (Mettler Toledo, Columbus, OH, USA) was used for thermo-gravimetric analysis (TGA) under nitrogen from 25 to 700 °C at 10 K/min. A sample mass of about 3 mg contained in a 70 μL alumina crucible was used for each measurement.

Contact angle data were acquired by sessile tests at RT based on the Young–Laplace equation using an Attension Theta Lite instrument (Biolin Scientific UK, Manchester, UK). Contact angle values at 0 s and 60 s (θ_{c0s} and θ_{c60s}, respectively) were acquired for each sample.

Dynamic mechanical thermal analysis (DMTA) was undertaken using a Tritec 2000 DMA instrument (Triton Technology Ltd, Nottinghamshire, UK) in tension mode with a sample length of 10 mm. Temperature scans were carried out from −100 to 110 °C at a heating rate of 2 K/min, a frequency of 1 Hz, and a displacement of 0.02 mm. The dynamic storage modulus (E'), loss modulus (E''), and loss tangent (tan $\delta = E''/E'$) were automatically calculated by the software program.

3. Results and discussion

The SEM images (Figure 1) show that both MMT and SPT were agglomerated (at this magnification) with diameters up to 30 µm. SPT was also bundled as needle-like nanostructures [23,27–29]. Chitosan was in the form of agglomerates with diameters up to about 200 µm and as fibrous structures as long as a few hundred µm (more images not shown here). SP formed globules with holes of different sizes on the surface and a hollow inside with a particle diameter ranging from about 10 µm to 130 µm (more images not shown here). These original structural features of biopolymers were destroyed by processing, resulting in cohesive materials.

Figure 2 displays the STEM images of the different samples. By way of example, for M1/M, both STEM-BF and STEM-HAADF images and a high magnification STEM-HAADF image are shown where, only STEM-BF images are shown for the other composite samples. Since HAADF images

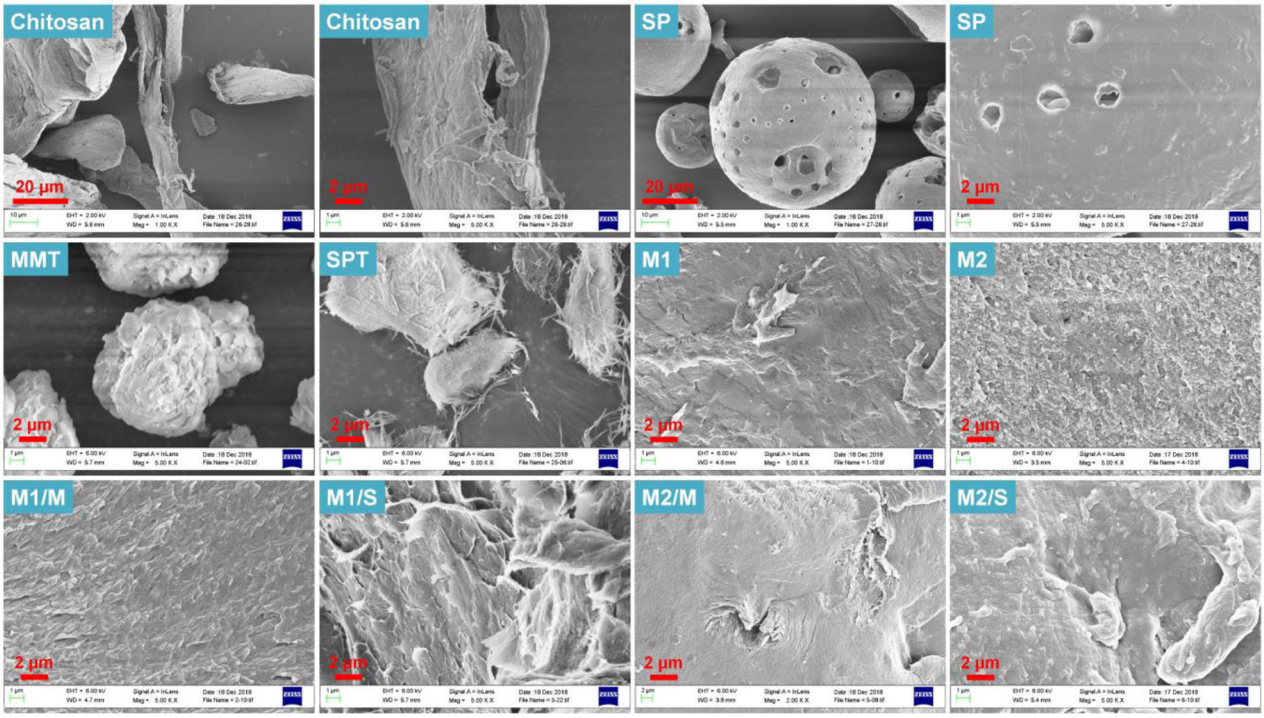

Figure 1. Scanning electron microscopy (SEM) images of chitosan, SP, MMT, and SPT, as well as cryo-fractured surfaces of the different biopolymer-based films.

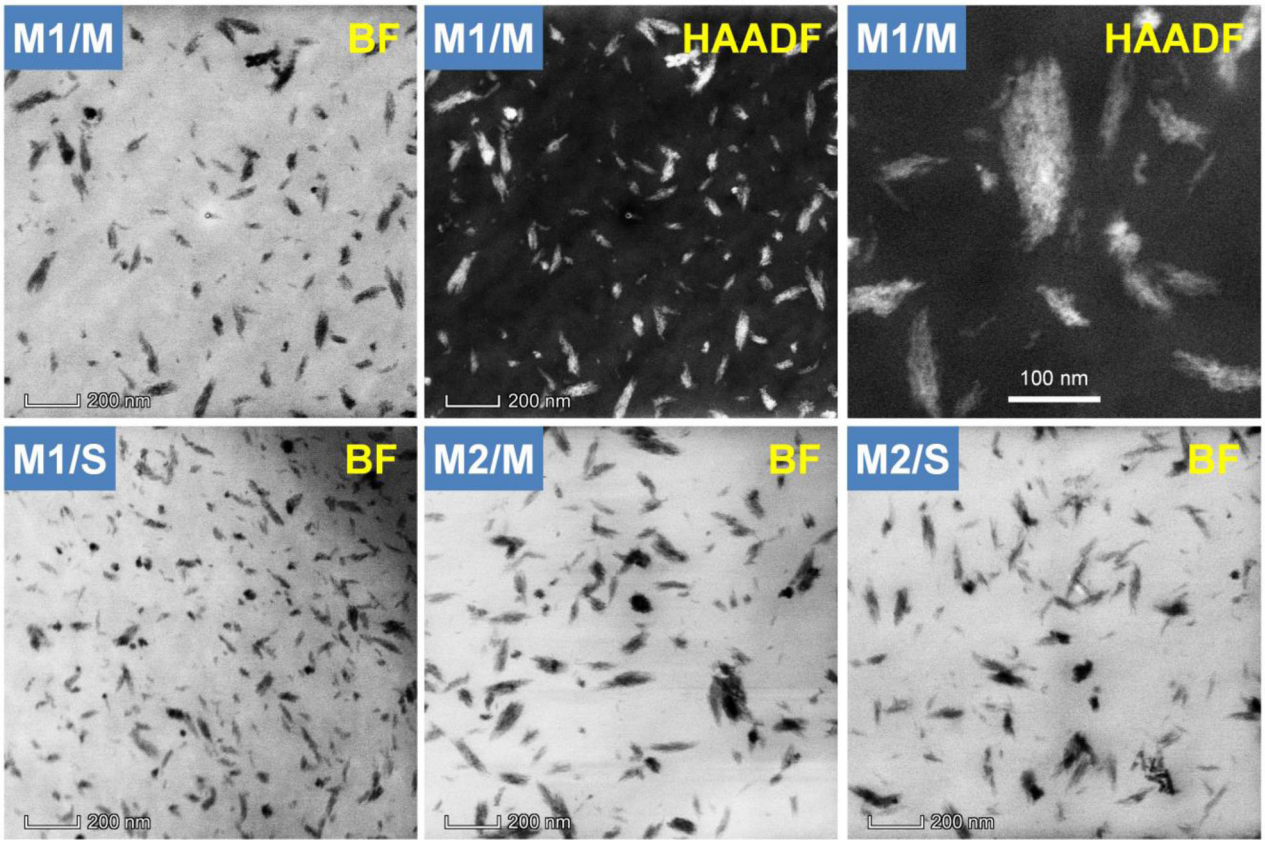

Figure 2. Scanning transmission electron microscopy (STEM) images of the different biopolymer-based films. BF, bright field; HAADF, high-angle annular dark field.

reveal mass-thickness contrast [30], the MMT (or SPT) appear bright in the images and vice versa the clay particles are seen as black or deep grey in the STEM-BF images. The processing protocol adopted in this work achieved excellent nanoclay dispersion in both the chitosan and chitosan/SP matrices, for all samples.

For the chitosan/SP matrix, it is apparent that the two biopolymers were homogeneously mixed as no fine-scale 'domains' were observed in the STEM

images, consistent with the observations made from SEM imaging. Hydrogen bonding has been considered to occur between chitosan and SF [9,13,14,31] and this should also be the case for the chitosan/SP matrix here.

The STEM images of M1/M show that the MMT generally has a size of <200 nm in length and <50 nm in width. In contrast, SPT in chitosan (M1/S) presents a relatively elongated shape (bundles of needles), although they are comparable to the MMT in size. The shear stress applied during thermochemical processing could physically break down the nanoclay agglomerates. Moreover, the use of chitosan/SP as the matrix instead of chitosan only resulted in more agglomerates and poorer dispersion of either MMT or SPT particles. It is likely, the introduction of the low-molecular-mass SP phase reduced the viscosity of the polymer matrix, resulting in lower shear stress during processing, leading to less effective dispersion of the clay particles.

Using XRD, the crystalline structures of chitosan, SP, MMT, SPT, and the different processed biopolymer films were examined (Figure 3). Chitosan displayed two major peaks at about 12.0° and 23.3° 2θ [17,32]. The peak at 12.0° ((020) reflection, d-spacing = 0.86 nm) is assigned to the hydrated crystals due to the integration of water molecules in the crystal lattice; and the peak located at 23.3° 2θ ((100) reflection, d-spacing = 0.44 nm) is attributed to the regular crystal lattice of chitosan [33]. SP displayed a sharp peak at 23.8° 2θ (d-spacing = 0.43 nm) and smaller peaks at 2θ angles of 18.4° (0.56 nm), 25.7° (0.40 nm), 32.9° (0.32 nm), and 37.4° (0.28 nm). These peaks are characteristic of the silk I structure [34,35], while some undefined crystalline structure may also exist.

MMT has a reflection peak at 10.3° 2θ, corresponding to a d_{001} basal spacing of 1.00 nm [36–41]. SPT showed a characteristic (110) peak at 8.5° 2θ, corresponding to a d-spacing of 1.21 nm [42–44]. This peak is associated with the typical feature of zeolitic pores inside the SPT needles formed by covalent bonds, which generally cannot be altered by processing [42,44].

Similar to the case for unprocessed chitosan, M1, M1/M, and M1/S had XRD curves with two apparent peaks at about 12.0° and 23.6° 2θ, although the intensities of these peaks were less than that obtained for unprocessed chitosan. In addition, for all chitosan films, there was a peak at 26.2° 2θ ((110) reflection, d-spacing = 0.39 nm), which was also observed previously for thermally processed chitosan [17,18,32,33]. This XRD reflection could also be attributed to the crystal lattice of chitosan [33].

As M1/M did not show the characteristic MMT peak at 10.3° 2θ, the MMT layers were delaminated by the processing step. MMT platelets are negatively charged and have a hydrophilic character [22]. Chitosan, a polycation under acidic conditions, could effectively interact with the negatively charged layers of MMT, functioning as an organomodifier (surfactant) [22,25]. Therefore, a high affinity between the chitosan matrix and MMT results from

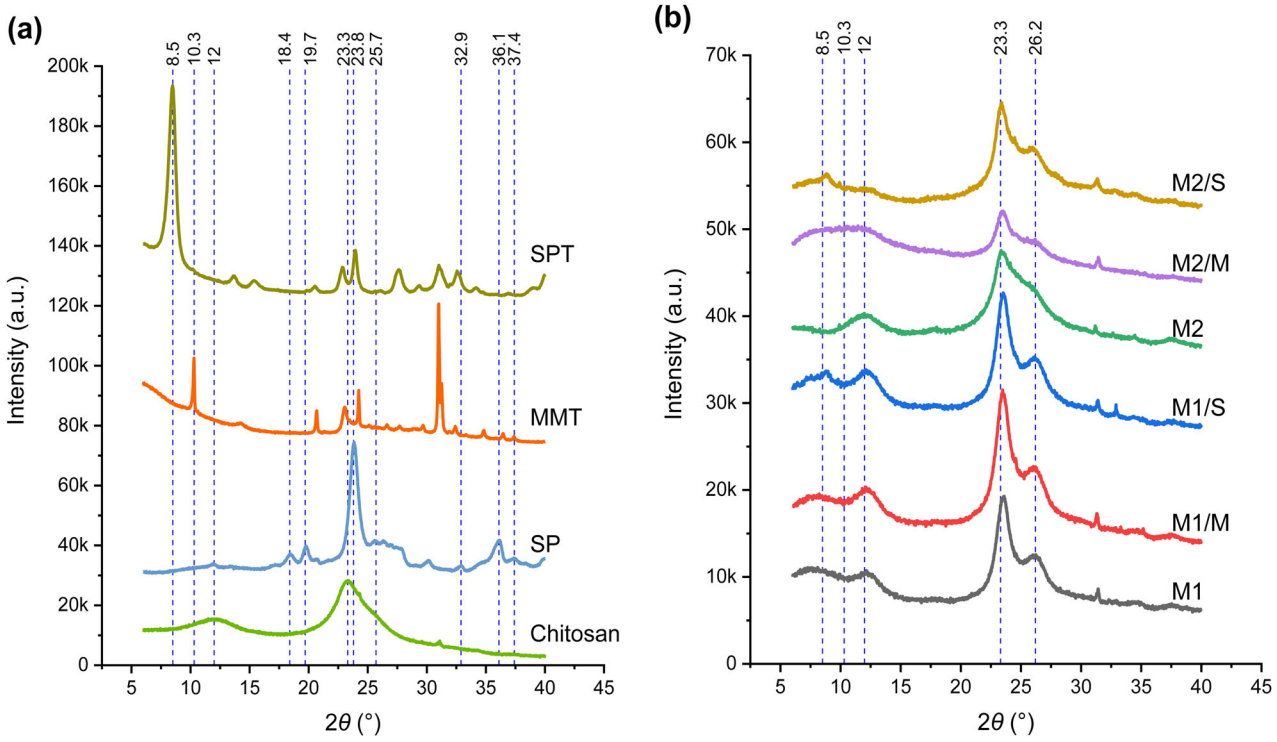

Figure 3. X-ray diffractograms for (a) chitosan, SP, MMT, SPT and (b) the different biopolymer-based films. The reference line indicates the characteristic peak positions of chitosan (12°, 23.3°, and 26.2°), SP (17°, 18.4°, 19.7°, 23.8°, 25.7°, 32.9°, 36.1°, and 37.4°), MMT (10.3°), and SPT (8.5°).

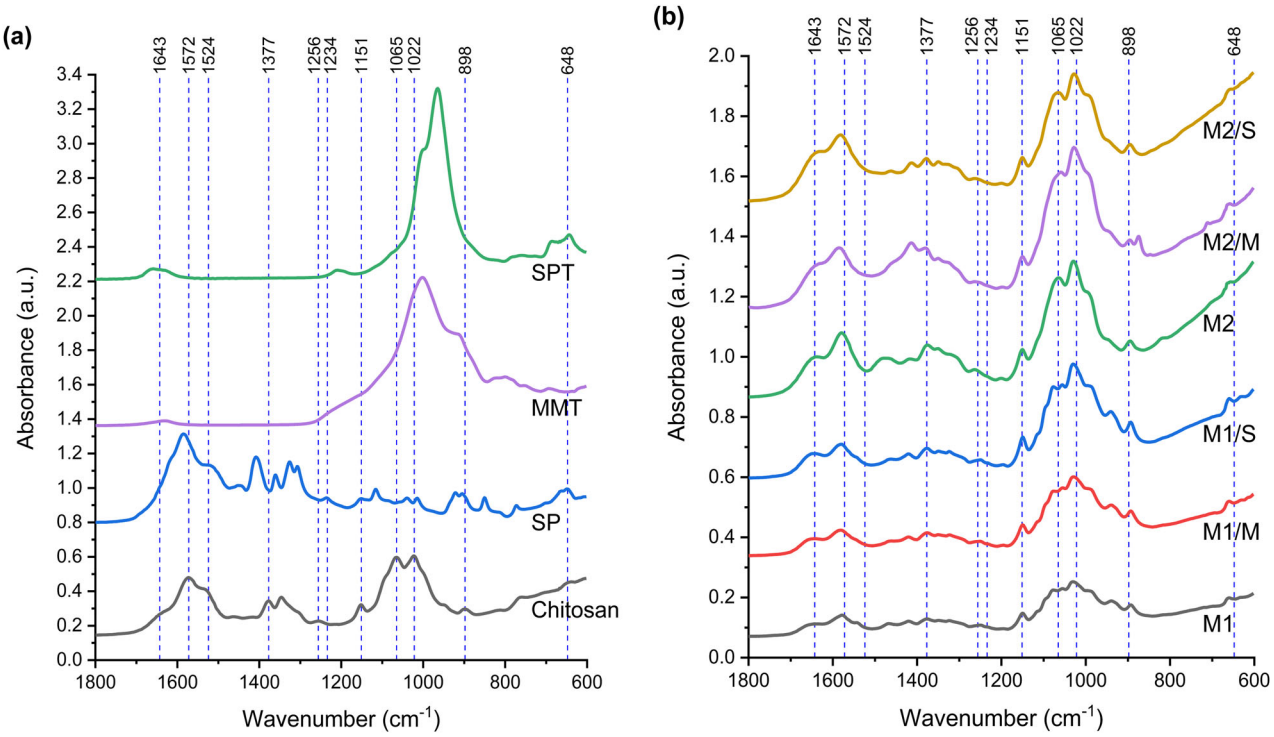

Figure 4. Fourier transform infrared (FTIR) spectra for (a) chitosan, SP, MMT, SPT and (b) the different biopolymer-based films. The references lines indicate the characteristic peak positions of chitosan (1643 cm^{-1}, 1,572 cm^{-1}, 1,377 cm^{-1}, 1,256 cm^{-1}, 1,151 cm^{-1}, 1,065 cm^{-1}, 1,022 cm^{-1}, and 898 cm^{-1}) and SP (1524 cm^{-1}, 1,234 cm^{-1}, and 648 cm^{-1}).

electrostatic and hydrogen-bonding interactions and, thus, excellent dispersion of MMT nanoplatelets in chitosan could be expected. In contrast, the characteristic peak of SPT at 8.5° 2θ is still present in the XRD pattern of M1/S, although at a slightly higher angle (8.8° 2θ), associated with the non-swelling nature of SPT (i.e. the zeolitic pores could not be affected by processing) [42,44]. Since SPT is also negatively charged [23,24], protonated chitosan, which is positively charged, can also strongly interact with SPT via electrostatic attraction and hydrogen bonding. Due to these interactions, chitosan molecules may even enter the zeolitic channels, resulting in slightly decreased channel spacing.

For M2, the characteristic chitosan peaks at 12.0°, 23.3° and 26.2° 2θ were still apparent. No SP features were evident, suggesting its original structure was completely destroyed by processing. M2/S also showed the characteristic SPT peak at 8.5° 2θ as was the case for M1/S. Compared with M2/S, M2/M displayed less intense reflections at 23.3° and 26.2° 2θ, suggesting that the re-crystallization of chitosan was inhibited to some extent by the presence of MMT. Moreover, the (001)-reflection of MMT was not observable for M2/M, indicating sufficient delamination of MMT.

FTIR analysis was undertaken in an attempt to understand the molecular interactions between the components of the biopolymer films (Figure 4). The characteristic absorption bands for chitosan, SP, MMT, and SPT are summarized in Table 2.

From Figure 4(b), it can be seen that M1, M1/M, and M1/S displayed similar FTIR spectra. The characteristic peaks of unprocessed chitosan were largely maintained but shifts in peak position could be seen. The significant change to the doublet at 1065 cm^{-1} (representing asymmetric C–O–C stretching in the glycosidic linkage) and 1022 cm^{-1} (–C–O– stretching of glucosamine) may be due to the disruption of the original chitosan structure. The peak at 1572 cm^{-1} (amide II or the amino group of chitosan) underwent a blue shift especially with inclusion of the nanoclays. The peak at 1256 cm^{-1} (amide III) was slightly red-shifted. In this regard, the amino (–NH_2) and amide (containing –NH–) groups should be involved in hydrogen-bonding interaction for the processed materials.

M2, M2/M, and M2/S all showed strong characteristic FTIR bands associated with chitosan, whereas the characteristic peaks of SP were not apparent. The characteristic amino and amide bands of SP may combine with those of chitosan. The intermolecular hydrogen-bonding interaction between the two biopolymers should be associated with the amide groups (containing –NH–) of SP and the carbonyl (C═O) and amino (–NH_2) groups of chitosan (not 100% deacetylated) [9,13,14,31]. This could also be demonstrated by a greater shift of the peak at 1572 cm^{-1} for M2 than for M1. For chitosan/SP matrix, inclusion of MMT resulted in a greater peak shift, indicating strong interactions between chitosan and MMT.

Table 2. FTIR bands and assignments.

Bands (cm^{-1})	Assignment	Refs
Chitosan		
1190–920 cm^{-1}	C–N stretching	[45]
1150–1040 cm^{-1}	Asymmetric C–O–C stretching in glycosidic linkage	[46]
1022 cm^{-1}	Skeletal vibration (–C–O– stretching) of glucosamine	[13,45,47]
1643 cm^{-1}	Amide I	[9,14,16,31,45–51]
1572 cm^{-1}	Amide II; Amino group ($–NH_2$) of chitosan	[9,14,16,31,45–51]
1256 cm^{-1}	Amide III	[9,14,16,31,47–51]
1377 cm^{-1}	CH_3 symmetrical deformation mode	[45,46,48,51]
SP		
1585 cm^{-1}	N–H bending of primary and secondary amines	[35,52–54]
1524 cm^{-1}	Amide II (random coil structure)	[35,52–54]
1234 cm^{-1}	Amide III (random coil structure)	[35,52–54]
640–644 cm^{-1}	Amide V (random coil structure)	[35,52–54]
MMT		
1001 cm^{-1}	Si–O stretching	[25,55,56]
1632 cm^{-1}	H–O–H deformation of the interlayer H_2O	[25,55,56]
SPT		
964 cm^{-1} and 1,029 cm^{-1}	Stretching of Si–O in the Si–O–Si groups of the tetrahedral sheet	[28,57,58]
1659 cm^{-1}	O–H stretching, from bound water coordinated to magnesium in the octahedral sheet	[28,57,58]

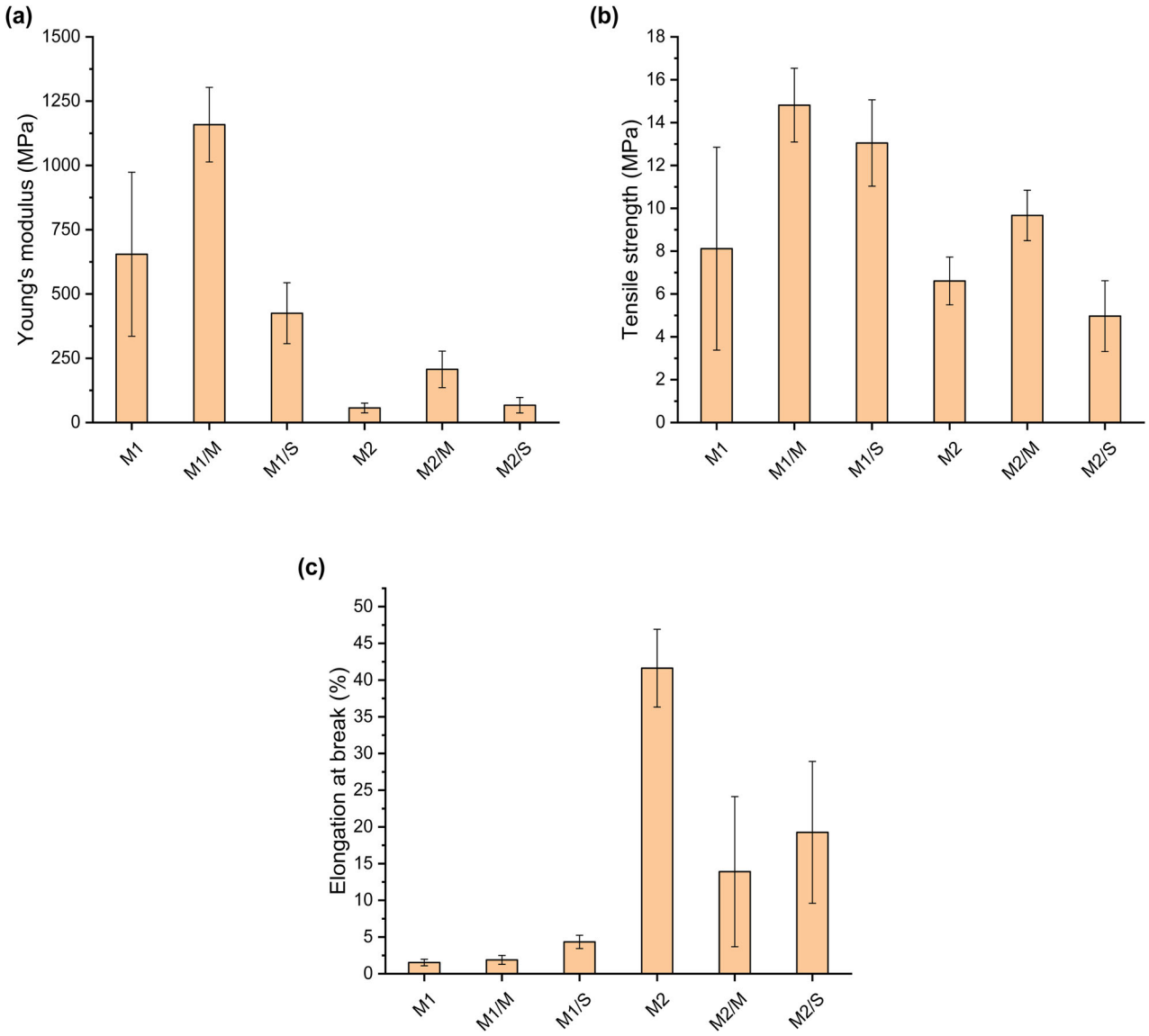

Figure 5. Mechanical properties (a) Young's modulus, (b) tensile strength, and (c) elongation at break of the different biopolymer-based films. The error bars represent standard deviations.

Figure 5shows the mechanical properties of the different biopolymer films. Overall, inclusion of MMT and SP strongly affected the σ_t, E, and ε_b of the biopolymer films. Compared with M1, M1/M displayed significantly increased E (from 654 ± 319 MPa to 1159 ± 145 MPa) and σ_t (8.1 ± 4.7 MPa to 14.8 ± 1.7 MPa) but similar ε_b ($1.5 \pm 0.4\%$ to $1.9 \pm 0.6\%$). The reinforcement effect of MMT on thermomechanically

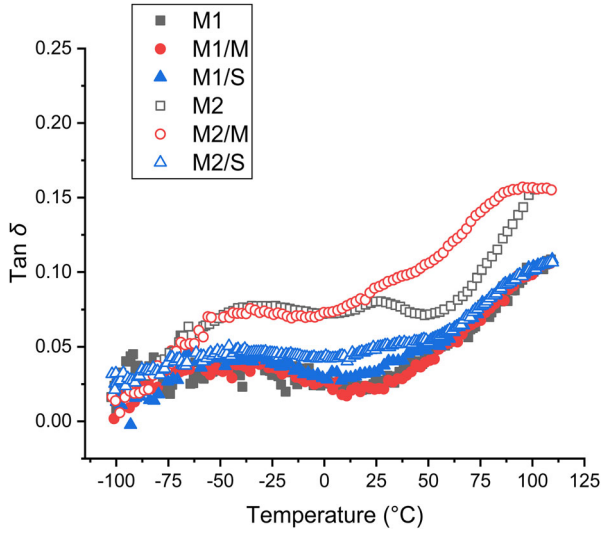

Figure 6. Loss tangent (tan δ) curves measured by dynamic mechanical thermal analysis (DMTA) for the different biopolymer-based films.

processed chitosan materials has also been reported previously [18]. Compared with M1, M1/S presented similar E (425 ± 118 MPa) and higher σ_t (13.0 ± 2.0 MPa) and ε_b (4.3 ± 0.9%). In this regard, compared with SPT nanoneedles, the larger surface area of rigid MMT nanosheets could result in more effective interfacial stress transfer and facilitate uniform stress distribution, leading to more enhanced mechanical properties. Moreover, all the chitosan films (M1, M1/M, and M1/S) had quite small ε_b values, indicating a brittle nature. This could also correspond to the high glass transition temperatures (T_g) of the biopolymer films (see Figure 6).

Compared with M1, M2 exhibited similar σ_t, lower E (56 ± 19 MPa) but largely increased ε_b (41.6 ± 5.3%). Therefore, the interaction of the low-molecular-mass SP with chitosan may have limited the interactions between chitosan chains (see FTIR results), leading to a plasticization effect. With inclusion of MMT, M2/M achieved a notable improvement in E (207 ± 71 MPa, 3.6 times that of M2) and σ_t (9.7 ± 1.2 MPa, 1.5 times that of M2) with reduced ε_b (13.9 ± 10.2%, 33% of that of M2). In contrast, inclusion of SPT did not afford any mechanical enhancement on the chitosan/SP matrix; in this case, the mechanical properties of the blend matrix could be predominately determined by the included SP. M2/S even displayed lower ε_b than M2 (19.3 ± 9.7%, 46% of that of M2). This, again, shows that SPT was not as effective as MMT in enhancing the mechanical properties of the biopolymer(s) and could even result in stress concentrators in the matrix possibly due to agglomeration of the nanoclay.

For composites of polymers and nanoclays, a modified Halpin–Tsai model has been proposed [59]:

$$E_c = E_m\left(\frac{1+2(\mathrm{MRF})\alpha\eta V_f}{1-\eta V_f}\right) \quad (1)$$

where E_c is the Young's modulus of the composite, E_m is the Young's modulus of the polymer matrix, α is aspect ratio, MRF is modulus reduction factor (0.66),

$$\eta = \frac{\frac{E_f}{E_m}-1}{\frac{E_f}{E_m}+2\alpha} \quad (2)$$

and

$$V_f = \frac{\frac{w_f}{\rho_f}}{\frac{w_f}{\rho_f}+\frac{(1-w_f)}{\rho_m}} \quad (3)$$

Equation (3) converts weight fraction of the filler (w_f) into volume fraction (V_f) based on the densities of the filler and the matrix (ρ_f and ρ_m, respectively). With $E_f \approx 170$ GPa, $\alpha \approx 28$ [59], ρ_f for MMT = 1.9 g/cm^3, and ρ_m for the biopolymer matrix assumed to be 1.2 g/cm^3, E_c can be estimated to be 846 MPa for M1/M and 76 MPa for M2/M, which are lower than the experimental E values of these two composites, 1159 MPa and 207 MPa, respectively. In this regard, the increase in E with addition of a nanofiller is not due to a single reinforcement effect but is also impacted by the variation in hydrogen-bonding between biopolymer chains [60].

The thermal stability of the different biopolymer films was studied using TGA with the plots of weight as a function of temperature shown in Figure 7(a,b). It can be seen that MMT and SPT were quite thermally stable until the end of measurement (700 °C) while chitosan, SP, and the different biopolymer films started a major weight loss after about 200 °C.

For better examining the degradation steps, the plots of derivative weight as a function of temperature were shown in Figure 7(c). For chitosan, there was a large thermal decomposition peak spanning from about 200 °C to 400 °C, with a peak maximum (T_d) at 296 °C, in agreement with previous reports [18,26,32]. SP displayed a broad thermal decomposition peak starting from about 130 °C and ending at 470 °C, with a doublet of peaks at 221 °C and 232 °C [26], which is most likely related to the breakage of peptide bonds (de-polymerization) and the pyrolysis of the de-polymerized products [9]. Heating to 700 °C did not result in a major weight loss for MMT or SPT. For both nanoclays, there was evaporation of free moisture and/or zeolitic water before 100 °C and, for SPT, a loss of coordinated water between 200 °C and 290 °C [61].

Like chitosan, M1 displayed one major weight loss with T_d = 274 °C, some 22 °C lower than that of chitosan itself. Additionally, there was a small shoulder process at about 230 °C, which might be due to the de-polymerization of chitosan. The decreased thermal stability of processed chitosan could be ascribed to the lower crystalline content and/or reduced molecular weight resulting from thermomechanical

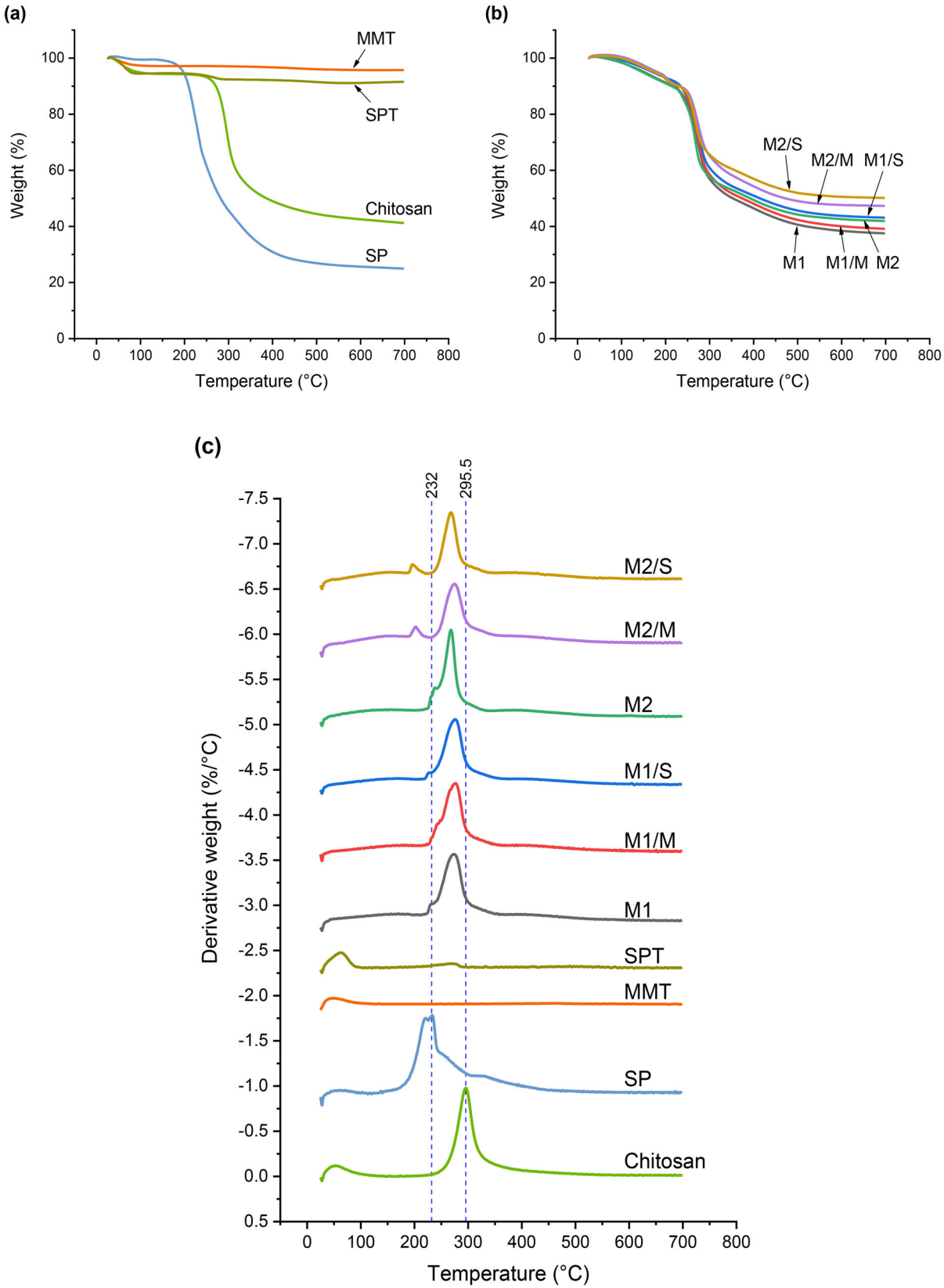

Figure 7. (a) and (b) Weight vs. temperature and (c) Derivative weight vs. temperature curves for chitosan, SP, MMT, SPT, and the different biopolymer-based films. The reference line in (c) indicates the maximum thermal decomposition temperature of SP and chitosan, respectively.

processing. Compared with M1, M1/M and M1/S did not show variation to T_d (remaining at 276 °C).

M2 also had a major weight loss with T_d at 268 °C and a small shoulder at 239 °C, attributed to the main decomposition step and initial depolymerization, respectively. The thermal decomposition of individual biopolymers is not identifiable, suggesting strong interactions between chitosan and SP. However, T_d was 5 °C lower than that for M1, suggesting the thermal stability of chitosan was

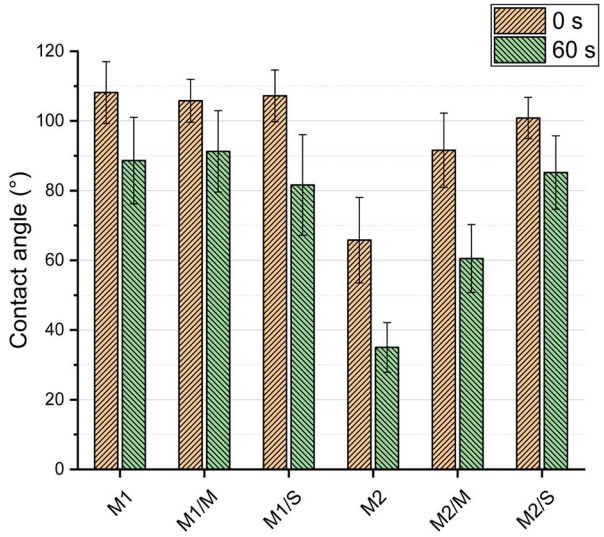

Figure 8. Contact angle values for the different biopolymer-based films at 0 s and 60 s. The error bars represent standard deviations.

reduced slightly by addition of SP. M2/S did not display any improvement in thermal stability as T_d remained unchanged at 268 °C. In comparison, for M2/M, T_d increased to 275 °C, similar to that for the chitosan films (M1, M1/M, and M1/S). This enhancement can be attributed to the layered structure of MMT, which could effectively retard the transfer to pyrolysis products [62,63].

Surface wettability (hydrophilicity/hydrophobicity) is particularly important for biocompatibility and cell adhesion [64]. Cell adhesion occurs preferentially on moderately water-wettable polymer surfaces [65]. Figure 8 shows the θ_{c0s} and θ_{c60s} values for the different films. M1, M1/M, and M1/S displayed similar θ_{c0s} (106°–108°) and θ_{c60s} (82°–91°), suggesting a negligible effect of the nanoclays on the surface wettability of the chitosan film.

Compared with M1 ($\theta_{c0s} = 108 \pm 9°$ and $\theta_{c60s} = 89 \pm 12°$), M2 displayed significantly reduced θ_{c0s} ($66 \pm 12°$) and θ_{c60s} ($35 \pm 7°$), confirming that SP is much more hydrophilic than chitosan. This result is expected, as SP is water-soluble and, has silk I and random coil structures (see FTIR and XRD discussion sections). Inclusion of MMT to this system notably decreased hydrophilicity. For M2/M $\theta_{c0s} = 92 \pm 11°$ and $\theta_{c60s} = 61 \pm 10°$. For M2/S, the respective values are $101 \pm 6°$ and $85 \pm 11°$. Although MMTs are hydrophilic, they should be less hydrophilic than SP. Effective dispersion of the MMT could interrupt and restrict the interactions between the biopolymers and water. SPT was more effective at enhancing the surface hydrophobicity of the hybrid biopolymer films. As M1/S and M2/S had similar θ_{c0s} and θ_{c60s} values, SPT fully counteracted the increased surface hydrophilicity caused by SP.

4. Conclusions

Chitosan and chitosan/SP films were successfully prepared by thermomechanical processing. Morphological, XRD and FTIR results demonstrate compatibility and strong hydrogen bonding interactions between chitosan and SP. Blending SP with chitosan led to a material with greater elasticity despite reduced mechanical strength, as well as greater surface wettability and lower thermal stability. Excellent dispersion of MMT nanoplatelets and SPT nanoneedles in both chitosan and chitosan/SP matrices was demonstrated. For the chitosan matrix, both MMT and SPT resulted in increased mechanical properties with MMT being more effective probably due to its rigid 2D layered structure and high surface area, but both had minor effects on thermal stability and surface wettability of the biopolymer matrices. For the chitosan/SP matrix, inclusion of MMT resulted in increased mechanical properties and thermal stability. Nonetheless, SPT was more effective than MMT at reducing the surface hydrophilicity of chitosan/SP and SPT fully counteracted the increased surface hydrophilicity that results on inclusion of SP in the formulation. Thus, this work has shown that properties of chitosan can be modified by inclusion of SP or different nanoclays as a route to tailoring more desired properties (balanced hydrophilicity and mechanical properties) for high-value applications (e.g. antimicrobial wound healing and tissue engineering).

Disclosure statement

No potential conflict of interest was reported by the authors.

Funding

The authors acknowledge funding from the European Union's Horizon 2020 research and innovation programme under the Marie Skłodowska-Curie Grant Agreement No. 798225; the China Scholarship Council (CSC); and the Guangxi Key Laboratory for Polysaccharide Materials and Modification, Guangxi University for Nationalities, China under grant No. GXPSMM18ZD-02.

Notes on contributors

Pei Chen is an associate professor at South China Agricultural University. Her research focuses on the processing and modification of biomass and agricultural products for materials and food applications. She was a visiting scholar at WMG, the University of Warwick, UK from 2018 to 2019.

Fengwei Xie is currently a Marie Skłodowska-Curie Individual Fellow at WMG, the University of Warwick, UK. His research focuses on 'green'/bio-polymers for sustainability, environmental protection, people's better life and health. He investigates the mechanisms behind the relationship among processing, structure and properties/functionality of biopolymers and biocomposites.

Fengzai Tang completed his PhD degree at the University of Sydney, Australia in 2008. He currently works at WMG, the University of Warwick, UK as an Engineer in microscopy and nanoanalysis.

Tony McNally is Chair Professor in Nanocomposites and founder and, first Director of the International Institute for Nanocomposites Manufacturing (IINM) at WMG, the University of Warwick, UK. His research interests include composites of 0D/1D/2D nanomaterials and polymers, functionalization of nanomaterials, processing-structure-property relationships in polymer science, compatibilization of immiscible polymer blends, mechanochemistry, and polymer modified bitumen.

ORCID

Fengwei Xie http://orcid.org/0000-0002-2033-082X
Tony McNally http://orcid.org/0000-0001-5436-4211

References

1. Koh L-D, Cheng Y, Teng C-P, et al. Structures, mechanical properties and applications of silk fibroin materials. Prog Polym Sci. 2015;46:86–110.
2. Rinaudo M. Chitin and chitosan: properties and applications. Prog Polym Sci. 2006;31(7):603–632.
3. Anitha A, Sowmya S, Kumar PTS, et al. Chitin and chitosan in selected biomedical applications. Prog Polym Sci. 2014;39(9):1644–1667.
4. Gobin AS, Froude VE, Mathur AB. Structural and mechanical characteristics of silk fibroin and chitosan blend scaffolds for tissue regeneration. J Biomed Mater Res. 2005;74A(3):465–473.
5. Yu L, Dean K, Li L. Polymer blends and composites from renewable resources. Prog Polym Sci. 2006;31(6):576–602.
6. Imre B, Pukánszky B. Compatibilization in bio-based and biodegradable polymer blends. Eur Polym J. 2013;49(6):1215–1233.
7. Chen J-P, Chen S-H, Lai G-J. Preparation and characterization of biomimetic silk fibroin/chitosan composite nanofibers by electrospinning for osteoblasts culture. Nanoscale Res Lett. 2012;7(1):170.
8. Lima PAL, Resende CX, de Almeida Soares GD, et al. Preparation, characterization and biological test of 3D-scaffolds based on chitosan, fibroin and hydroxyapatite for bone tissue engineering. Mater Sci Eng C Mater Biol Appl. 2013;33(6):3389–3395.
9. Sionkowska A, Płanecka A. Preparation and characterization of silk fibroin/chitosan composite sponges for tissue engineering. J Mol Liq. 2013;178(Supplement C):5–14.
10. Zeng S, Liu L, Shi Y, et al. Characterization of silk fibroin/chitosan 3D porous scaffold and in vitro cytology. PLoS One. 2015;10(6):e0128658.
11. Vishwanath V, Pramanik K, Biswas A. Optimization and evaluation of silk fibroin–chitosan freeze-dried porous scaffolds for cartilage tissue engineering application. J Biomater Sci Polym Ed. 2016;27(7):657–674.
12. Kweon H, Ha HC, Um IC, et al. Physical properties of silk fibroin/chitosan blend films. J Appl Polym Sci. 2001;80(7):928–934.
13. Kweon H, Um IC, Park YH. Structural and thermal characteristics of *Antheraea pernyi* silk fibroin/chitosan blend film. Polymer. 2001;42(15):6651–6656.
14. Sionkowska A, Płanecka A. Surface properties of thin films based on the mixtures of chitosan and silk fibroin. J Mol Liq. 2013;186(Supplement C):157–162.
15. Nogueira GM, Swiston AJ, Beppu MM, et al. Layer-by-layer deposited chitosan/silk fibroin thin films with anisotropic nanofiber alignment. Langmuir. 2010;26(11):8953–8958.
16. Fernandez JG, Ingber DE. Unexpected strength and toughness in chitosan–fibroin laminates inspired by insect cuticle. Adv Mater Weinheim. 2012;24(4):480–484.
17. Epure V, Griffon M, Pollet E, et al. Structure and properties of glycerol-plasticized chitosan obtained by mechanical kneading. Carbohydr Polym. 2011;83(2):947–952.
18. Xie DF, Martino VP, Sangwan P, et al. Elaboration and properties of plasticised chitosan-based exfoliated nano-biocomposites. Polymer. 2013;54(14):3654–3662.
19. Zhang Y, Liu B-L, Wang L-J, et al. Preparation, structure and properties of acid aqueous solution plasticized thermoplastic chitosan. Polymers. 2019;11(5):818.
20. Gao C, Pollet E, Avérous L. Properties of glycerol-plasticized alginate films obtained by thermo-mechanical mixing. Food Hydrocolloids. 2017;63:414–420.
21. Rinaudo M, Pavlov G, Desbrières J. Influence of acetic acid concentration on the solubilization of chitosan. Polymer. 1999;40(25):7029–7032.
22. Chivrac F, Pollet E, Schmutz M, et al. New approach to elaborate exfoliated starch-based nanobiocomposites. Biomacromolecules. 2008;9(3):896–900.
23. Chivrac F, Pollet E, Schmutz M, et al. Starch nanobiocomposites based on needle-like sepiolite clays. Carbohydr. Polym. 2010;80(1):145–153.
24. Darder M, López-Blanco M, Aranda P, et al. Microfibrous chitosan – sepiolite nanocomposites. Chem Mater. 2006;18(6):1602–1610.
25. Darder M, Colilla M, Ruiz-Hitzky E. Biopolymer – clay nanocomposites based on chitosan intercalated in montmorillonite. Chem Mater. 2003;15(20):3774–3780.
26. Meng L, Xie F, Zhang B, et al. Natural biopolymer alloys with superior mechanical properties. ACS Sustain Chem Eng. 2019;7(2):2792–2802.
27. Duquesne E, Moins S, Alexandre M, et al. How can nanohybrids enhance polyester/sepiolite nanocomposite properties? Macromol Chem Phys. 2007;208(23):2542–2550.
28. Soheilmoghaddam M, Wahit MU, Yussuf AA, et al. Characterization of bio regenerated cellulose/sepiolite nanocomposite films prepared via ionic liquid. Polym Test. 2014;33:121–130.
29. de Lima JA, Camilo FF, Faez R, et al. A new approch to sepiolite dispersion by treatment with ionic liquids. Appl Clay Sci. 2017;143:234–240.
30. Williams DB, Carter CB. Amplitude contrast. In: Williams DB, Carter CB, editors. Transmission electron microscopy: a textbook for materials science. Boston, MA: Springer US, 2009. pp. 371–388.
31. Chen X, Li W, Zhong W, et al. pH sensitivity and ion sensitivity of hydrogels based on complex-

forming chitosan/silk fibroin interpenetrating polymer network. J Appl Polym Sci. 1997;65(11):2257–2262.
32. Matet M, Heuzey M-C, Pollet E, et al. Innovative thermoplastic chitosan obtained by thermo-mechanical mixing with polyol plasticizers. Carbohydr Polym. 2013;95(1):241–251.
33. Kittur FS, Vishu Kumar AB, Tharanathan RN. Low molecular weight chitosans—preparation by depolymerization with *Aspergillus niger* pectinase, and characterization. Carbohydr Res. 2003;338(12):1283–1290.
34. Jin H-J, Kaplan DL. Mechanism of silk processing in insects and spiders. Nature. 2003;424(6952):1057–1061.
35. Lu Q, Hu X, Wang X, et al. Water-insoluble silk films with silk I structure. Acta Biomater. 2010;6(4):1380–1387.
36. Dean KM, Do MD, Petinakis E, et al. Key interactions in biodegradable thermoplastic starch/poly(vinyl alcohol)/montmorillonite micro- and nanocomposites. Compos Sci Technol. 2008;68(6):1453–1462.
37. Dai H, Chang P, Geng F, et al. Preparation and properties of thermoplastic starch/montmorillonite nanocomposite using *N*-(2-hydroxyethyl)formamide as a new additive. J Polym Environ. 2009;17(4):225–232.
38. Wang N, Zhang X, Han N, et al. Effect of citric acid and processing on the performance of thermoplastic starch/montmorillonite nanocomposites. Carbohydr Polym. 2009;76(1):68–73.
39. Wang N, Zhang X, Wang X, et al. Ionic liquids modified montmorillonite/thermoplastic starch nanocomposites as ionic conducting biopolymer. Macromol Res. 2009;17(5):285–288.
40. Arroyo OH, Huneault MA, Favis BD, et al. Processing and properties of PLA/thermoplastic starch/montmorillonite nanocomposites. Polym Compos. 2010;31(1):114–127.
41. Wang N, Zhang X, Han N, et al. A facile method for preparation of thermoplastic starch/urea modified montmorillonite nanocomposites. J Compos Mater. 2010;44(1):27–39.
42. Benlikaya R, Alkan M, Kaya İ. Preparation and characterization of sepiolite-poly(ethyl methacrylate) and poly(2-hydroxyethyl methacrylate) nanocomposites. Polym Compos. 2009;30(11):1585–1594.
43. Tartaglione G, Tabuani D, Camino G, et al. PP and PBT composites filled with sepiolite: morphology and thermal behaviour. Compos Sci Technol. 2008;68(2):451–460.
44. Chen H, Zheng M, Sun H, et al. Characterization and properties of sepiolite/polyurethane nanocomposites. Mater. Sci Eng A. 2007;445–446:725–730.
45. Lawrie G, Keen I, Drew B, et al. Interactions between alginate and chitosan biopolymers characterized using FTIR and XPS. Biomacromolecules. 2007;8(8):2533–2541.
46. Pawlak A, Mucha M. Thermogravimetric and FTIR studies of chitosan blends. Thermochim Acta. 2003;396(1–2):153–166.
47. Kim HS, Kim JT, Jung YJ, et al. Preparation of a porous chitosan/fibroin-hydroxyapatite composite matrix for tissue engineering. Macromol Res. 2007;15(1):65–73.
48. Sannan T, Kurita K, Ogura K, et al. Studies on chitin: 7. IR spectroscopic determination of degree of deacetylation. Polymer. 1978;19(4):458–459.
49. Brugnerotto J, Lizardi J, Goycoolea FM, et al. An infrared investigation in relation with chitin and chitosan characterization. Polymer. 2001;42(8):3569–3580.
50. Chen X, Li W, Yu T. Conformation transition of silk fibroin induced by blending chitosan. J Polym Sci B Polym Phys. 1997;35(14):2293–2296.
51. Chen Z, Mo X, He C, et al. Intermolecular interactions in electrospun collagen–chitosan complex nanofibers. Carbohydr Polym. 2008;72(3):410–418.
52. Tsukada M, Gotoh Y, Nagura M, et al. Structural changes of silk fibroin membranes induced by immersion in methanol aqueous solutions. J Polym Sci B Polym Phys. 1994;32(5):961–968.
53. Um IC, Kweon H, Park YH, et al. Structural characteristics and properties of the regenerated silk fibroin prepared from formic acid. Int J Biol Macromol. 2001;29(2):91–97.
54. Jin H-J, Park J, Karageorgiou V, et al. Water-stable silk films with reduced β-sheet content. Adv Funct Mater. 2005;15(8):1241–1247.
55. Bukka K, Miller JD, Shabtai J. FTIR study of deuterated montmorillonites: structural features relevant to pillared clay stability. Clays Clay Miner. 1992;40(1):92–102.
56. Chen G, Liu S, Chen S, et al. FTIR spectra, thermal properties, and dispersibility of a polystyrene/montmorillonite nanocomposite. Macromol Chem Phys. 2001;202(7):1189–1193.
57. Alkan M, Tekin G, Namli H. FTIR and zeta potential measurements of sepiolite treated with some organosilanes. Microporous Mesoporous Mater. 2005;84(1–3):75–83.
58. Sabah E, Çelik MS. Interaction of pyridine derivatives with sepiolite. J Colloid Interface Sci. 2002;251(1):33–38.
59. Mohapatra AK, Mohanty S, Nayak SK. Modeling of the mechanical properties of polylactic acid/clay nanocomposites using composite theories. Int J Plast Technol. 2011;15(2):174–187.
60. Kelnar I, Kovářová J, Tishchenko G, et al. Chitosan/chitin nanowhiskers composites: effect of plasticisers on the mechanical behaviour. J Polym Res. 2015;22(2):5.
61. Tartaglione G, Tabuani D, Camino G. Thermal and morphological characterisation of organically modified sepiolite. Microporous Mesoporous Mater. 2008;107(1–2):161–168.
62. Wang SF, Shen L, Tong YJ, et al. Biopolymer chitosan/montmorillonite nanocomposites: preparation and characterization. Polym Degrad Stab. 2005;90(1):123–131.
63. Wang S, Chen L, Tong Y. Structure–property relationship in chitosan-based biopolymer/montmorillonite nanocomposites. J Polym Sci Part A: Polym Chem. 2006;44(1):686–696.
64. Kim MS, Khang G, Lee HB. Gradient polymer surfaces for biomedical applications. Prog Polym Sci. 2008;33(1):138–164.
65. van Wachem PB, Beugeling T, Feijen J, et al. Interaction of cultured human endothelial cells with polymeric surfaces of different wettabilities. Biomaterials. 1985;6(6):403–408.